Single-Site Multi-Instrument Study of Peak Plasma Density in the Ionosphere

Mohamed O. Shammat[1], Bodo W. Reinisch[1,2], Ivan Galkin[1], Philip J. Erickson[3], Jay A. Weitzen[1], William C. Rideout[3]

[1]University of Massachusetts Lowell

[2]Lowell Digisonde International

[3]Haystack Observatory, Massachusetts Institute of Technology, Westford, MA

Corresponding author: Mohamed Shammat (mohamed_osman1@student.uml.edu)

†Additional author notes should be indicated with symbols (current addresses, for example).

Abstract

Unlike the conventional representations of the vertical electron density profile $N(h)$F2 of the F2 layer in the ionosphere around peak density N_mF2 by a single-maximum 'pointed-peak' function, this paper introduces the Peak Density Thickness (PDT) formalism, which allows the possibility for the plasma density at the peak to remain constant within an altitude interval χ. Several independent observations support such a 'broad-peak' or 'flat-nose' concept, including simultaneous measurements of the sub-peak and super-peak density profiles using different radar techniques. In particular, profile measurements obtained at the mid-latitude MIT Haystack observatory by the Millstone Hill Incoherent Scatter Radar (MH-ISR) reveal the presence and diurnal variation of PDT, ranging from ~ 0 km at nighttime to tens of km at midday. The PDT measurements by MH-ISR were coordinated with the Digisonde Portable Sounder DPS4D soundings of the sub-peak ionosphere up to h_mF2. Remarkable agreement of these independent measurements of the lower boundary of the χ interval, h_mF2, and the peak density, N_mF2, is observed compared to MH-ISR when its ion-line acoustic resonance scattering specification of $N(h)$ is complemented with an accurate F2 peak plasma-line ordinary Langmuir wave measurement of N_mF2 for the profile calibration. PDT remains highest during the afternoon hours before starting to decrease after sunset. Case studies demonstrate how PDT can be estimated from the Digisonde bottomside thickness parameter B0. Allowing for the flat-nose section χ in the F-region profile formalism will improve the accuracy of the topside specification deduced from ground-based ionosonde measurements.

1 Introduction

The generally accepted wisdom says that the Earth's ionosphere has a well-defined pointed peak of the ionized gas density due to opposing vertical trends in the ionizing Solar radiation and the atmospheric density (Fleming, 1902); the peak admits several formal "layer-like" representations that use various physics-based (e.g., Chapman, 1931) or numerical (e.g., the quasi-parabolic definition by Croft and Hoogansian, 1968) constructs. Such formal representations of the pointed peak shape have become quite common in academic literature and applications, albeit not always matching the observed properties of the ionosphere. A notable exception was reported in comparative studies by the coordinated bottomside and topside plasma specifications of the peak height h_mF2 using ground and spacecraft ionosondes. Although the observed O-wave critical frequency of the F2 layer, f_oF2, matched well during these ground-spacecraft conjunctions (meaning that the peak densities N_mF2 were in agreement), an apparent discontinuity in the virtual heights h' near f_oF2 provided by sub-peak and super-peak sounding (solid lines in Figure 1, after Jackson et al., 1980) was common, suggesting a gap between the sub- and super-peak heights h_mF2. Remarkably, despite the observed h' discontinuity, the combined N_e(h) profile representation of the observations (dashed curve in Figure 1) was still assumed to follow the commonly accepted layer formalism, even though it would lack physical justification.

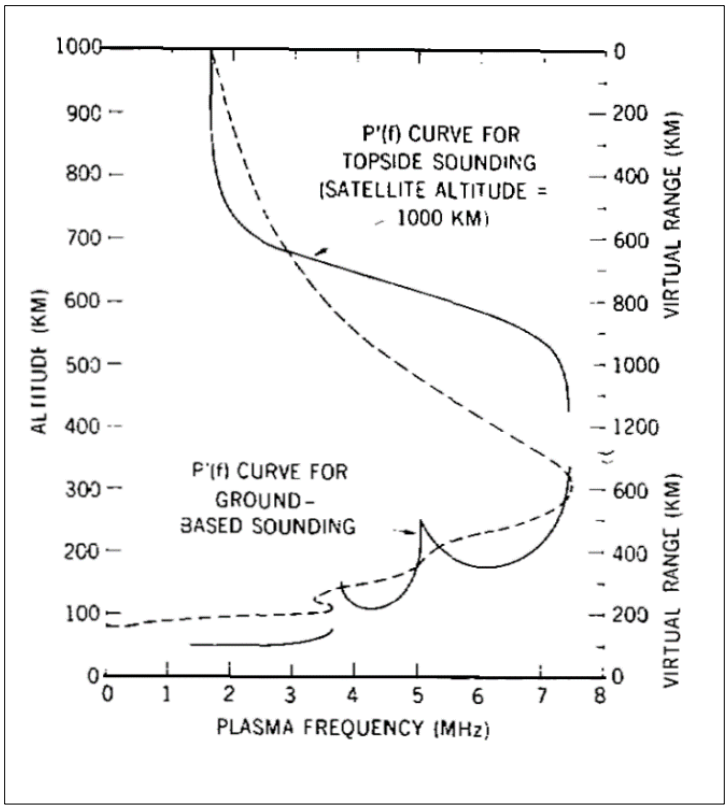

Figure 1. Reproduced figure (Jackson et al.,1980). Vertical electron profile (dashed line, left vertical axis) derived from the O-wave virtual ranges (heights) (solid lines, right vertical axis) as observed upward from the ground and downward from the satellite. Data are for 1651 GMT, June 10, 1968, Wallops Island, VA.

The disagreements between sub- and super-peak observations of h_mF2 have not been thoroughly investigated on a case-by-case basis in the literature due to the rare occurrences of such simultaneous measurements by spaceborne topside and ground-based bottomside ionosondes. A notable study of the monthly median h_mF2 values at mid-latitude locations in North America and Europe was conducted by Nsumei et al. (2010), in which ISIS-2 topside ionosonde measurements in 1973-1983 were compared to the ground-based ionosonde measurements 1-2 decades later. Statistically, a fair agreement of h_mF2 was reported by that comparative study, with the exception of spring evening hours when h_mF2(top) - h_mF2 (bottom) disagreement of medians reached ~100 km. By this date, the discrepancy remains unexplained and argued to be a possible artifact of the data acquisition or computation.

Another notable deviation from the commonly accepted peak density profile shape, as demonstrated in this paper, is seen in the unprocessed $N(h)$ profiles of the ionospheric plasma above and below h_mF2 provided by the Incoherent Scatter Radars (ISR). Open-data availability of the ionosonde and ISR measurements allows coordinated investigations of the peak density in the ionosphere with comparisons of the sub-peak and super-peak descriptions provided by collocated sensor instruments. One such investigation is presented here using the bottom- and topside profiles acquired by simultaneous measurements from the Millstone Hill ISR (MH-ISR)

(Evans, 1965; Erickson et al., 1998; 2012) and the collocated Digisonde DPS4D (Reinisch et al., 2009).

2 Data Acquisition, Selection, and Pre-processing

2.1 Millstone Hill ISR

Inspection of the profile shape in the area of the maximum plasma density in the ionosphere was possible using the vertical electron density profiles acquired by the Incoherent Scatter Radar (ISR) at Millstone Hill (MH), operating at MIT Haystack Observatory as part of the National Science Foundation's Millstone Hill Geospace Facility. MH-ISR measures the mid-latitude electron density profile from the E region up into the topside ionosphere. MH-ISR observes the ionosphere in a wide variety of experiment modes targeting different altitude regions. For the purpose of this investigation, two MH-ISR modes were used simultaneously to measure ionospheric parameters, including electron density: (M1) the ion-acoustic resonance that yields the vertical electron density profile $N(h)$, and (M2) the ordinary-wave Langmuir-mode plasma resonance technique that produces an accurate peak density N_mF2 value in addition to the entire M1-provided $N(h)$ profile. For brevity, we refer to the M1 mode as 'ion-line', and the M2 mode as 'plasma-line'.

Millstone Hill has operated since 1960 as a mid-latitude incoherent scatter radar facility, measuring the narrow bandwidth ion-line at E, F, and near topside regions. Beginning in 2015, software radio and radar technique advances allowed routine observation of the very weak plasma line resonance, located up to several MHz or more away from the ion-line center frequency at typical mid-latitude ionospheric electron densities. Accordingly, we searched in the Madrigal database for full Millstone Hill electron density profiles that would also include both bottomside and topside parts and that included both ion line and plasma line observations. Up until 2022, there are ~ 40 days where ion line full electron density profile measurements were computed and archived. Of these experiments, only a few days have a continuous 24-hour timeline of the full profile due to facility funding limitations. June 22, 2016 is one of these days selected for this study.

The selected MH-ISR ion-line profiles on June 22nd, 2016, employed an alternating code with phase-modulated pulses (Lehtinen and Häggström, 1987) optimized to measure the bottomside and the lower topside electron density profiles with an effective altitude resolution of ~4.5 km in the E region, slowly increasing with altitude. For the plasma-line mode, we also selected the concurrent data measured around the exact same times the ion acoustic profiles were measured. The plasma-line measurements are only available in the daytime due to the need for the presence of photoelectrons which enhance the strength of the Langmuir mode to detectable levels (Showen, 1979). Therefore, we selected only daytime plasma-line N_mF2 for this study.

The main MH-ISR data products in the Madrigal databases undergo significant processing to form a calibrated, cleaned, verified Level 2 observation result. One of the commonly used Level-2 products in the Madrigal databases is subjected to so-called 'gridded data transformation', in which the electron density profile is averaged and fitted into a uniform 15-minute time cadence and a standard constant altitude grid with the fixed upper altitude boundary of 548 km. The MH-ISR gridded data transformation uses several techniques beyond the scope of this investigation, including a cubic spline fit that adheres to the classic pointed-peak profile shape at N_mF2 in order to produce the output product (Holt, 2008). Since we are

looking for deviations from the classic shape formalism, the MH-ISR source $N(h)$ profiles prior to their gridded transformation need to be retrieved from the Madrigal database. Not only do these records contain the profile information before averaging, calibrating, and rebinning, but also they are more likely to be simultaneous with collocated Digisonde measurements because of their instantaneous rather than 15-minute average nature. Also, the instantaneous ion line mode has higher altitude resolution compared to the gridded data mode, and this is useful for comparisons in this study.

Analysis of the source N_e profiles from MH-ISR requires significant instrument expertise. Figure 2 is an example of the overlaid source and binned profiles that illustrates the challenges of data analysis required to promote this data product to the next Level 2 category.

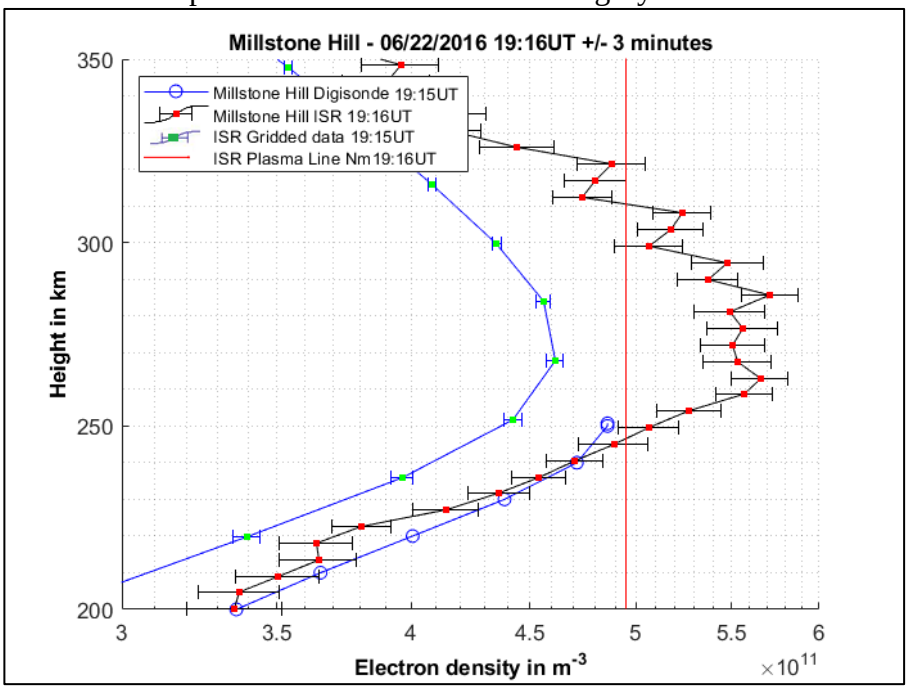

Figure 2. Comparison of the MH-ISR observed source $N(h)$ profile (red squares) derived using the ion-line analysis with the overlaid gridded-data 15-min average profile (green squares) and N_mF2 value provided by the plasma-line computation (vertical red line), and the Digisonde-observed bottomside $N_{bot}(h)$ profile (blue circles).

As seen in Figure 2, the peak density N_mF2 in the ion-line profile $N(h)$ disagrees with the plasma-line N_mF2, which necessitates $N(h)$ *recalibration* in this particular case. Here recalibration refers to a procedure of transforming the original ion-line $N(h)$ values so that their maximum value matches the accurate plasma-line N_mF2 reference. The recalibration procedure is illustrated in Figure 3. The original $N(h)$ profiles (the left column of Figure 3, panels (a) and (c), red squares) are shown prior to their standard calibration, averaging, and gridding to produce the Madrigal Level 2 data product (Holt, 2008). The right panels (b) and (d) display N_mF2-calibrated profiles after their 'elastic' transformation that, instead of simply shifting the profile to the lower densities, recognizes the proportionality of the overestimating to the ambient density. The elastic transformation algorithm starts by determining the value of N_mF2 derived from the ISR ion-line profile, and compares the N_mF2 value to the N_mF2 derived from the ISR plasma line. The

absolute difference is calculated and multiplied by a constant relaxation factor. The result of this product is subtracted from N_mF2 ion-line to produce the relaxation boundaries of the elastic transformation. A weighted shift is applied on the ion-line density profile within the relaxation boundaries and each point is shifted towards the plasma line N_mF2 value based on its absolute difference from the relaxation boundaries.

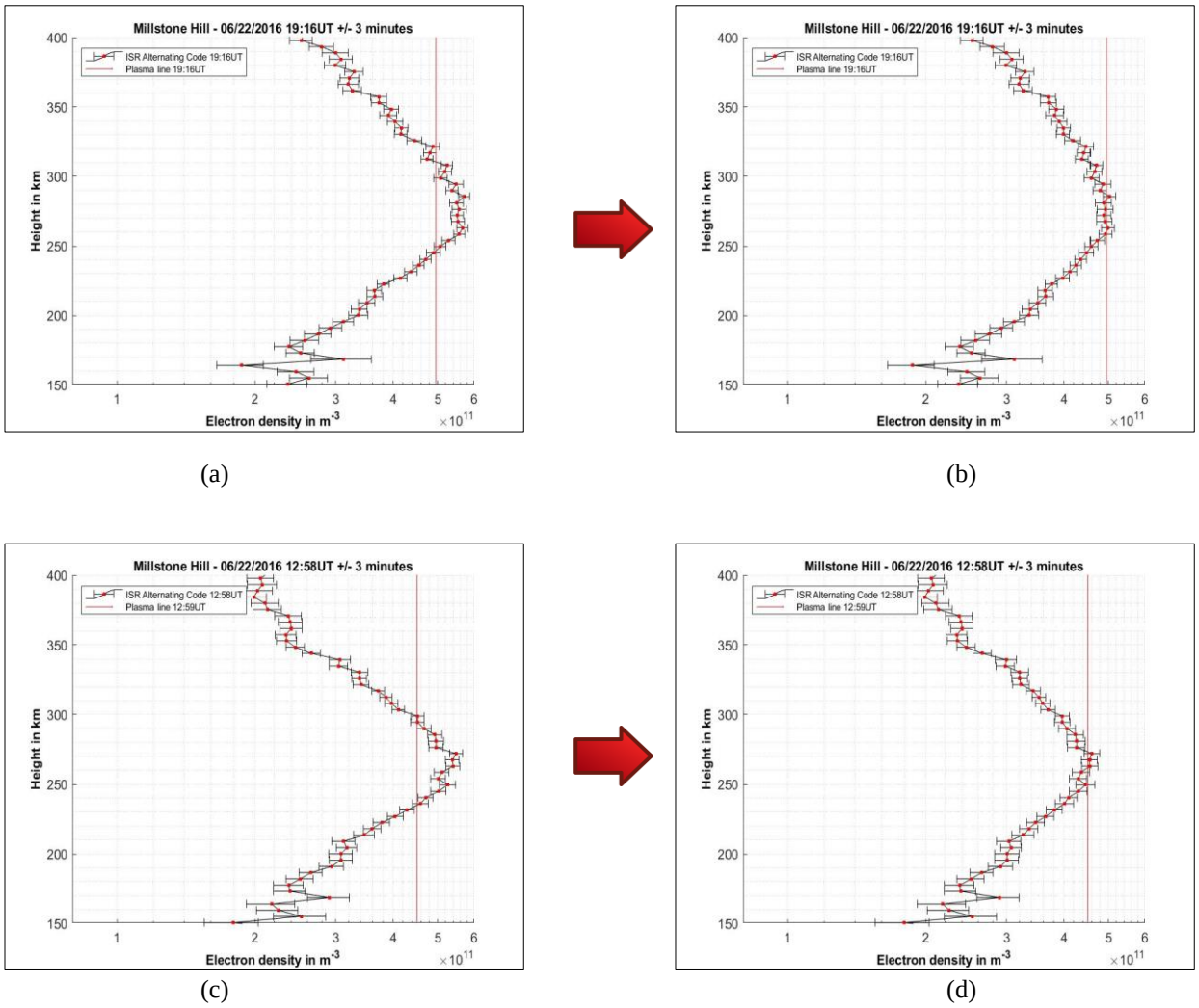

Figure 3. The original ISR ion-line electron density profile $N(h)$ (the left column, red squares) is elastically scaled to match the ISR plasma-line N_mF2 value (the vertical red lines) to produce the N_m-calibrated ion-line profile (the right column, red squares).

2.2 Millstone Hill Digisonde

Millstone Hill (MH) Digisonde bottomside profiles used in this study were retrieved from the Digital Ionogram Database (DIDBase) operated by the University of Massachusetts Lowell as a part of the Realistic Ionosphere project (Galkin et al., 2018) and its world-wide ionosonde network of the Global Ionosphere Radio Observatory (GIRO) (Reinisch and Galkin, 2011). All ionograms used in this study were manually validated using the software client "SAO Explorer"

with read/write access to DIDBase over the Internet (Khmyrov et al., 2008). The MH Digisonde has a large archived data collection at DIDBase, and since we are looking for simultaneous ISR measurements, our selection of the bottomside profiles was dictated by MH-ISR data availability. The example ionogram in Figure 4 was acquired on June 22, 2016, one day when 24-hour ISR measurements with full-altitude profiles were available.

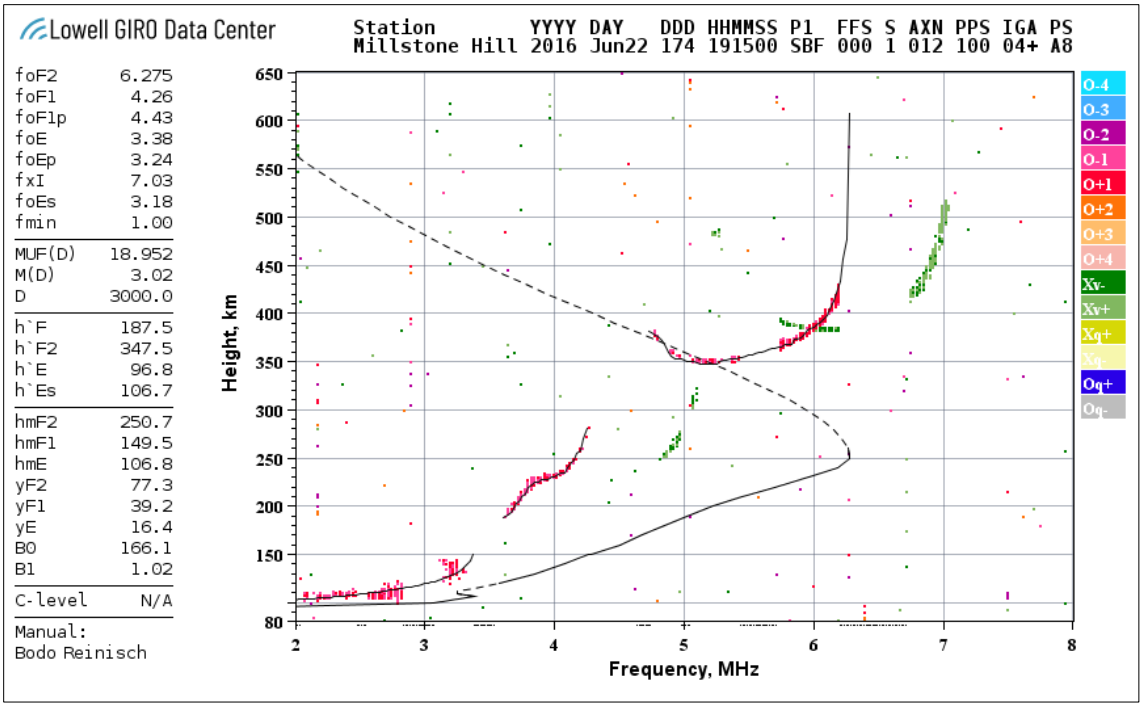

Figure 4. Manually scaled Digisonde ionogram on 2016/06/22 1915 UT, close to the time of the ISR measurement at 19:16 UT (Figure 2). The O-wave (red) and X-wave (green) echoes of the Digisonde transmissions form traces of the virtual height *h*'(*f*) as functions of the operating frequency *f; h'(f)* = ½ *t c* , where t is the measured pulse travel time, and c the free space speed of light. The O-wave *h*'(*f*) traces are scaled (thin black lines), to be then inverted to the true height profile *h*(*f*) (solid black line for observed data, and dashed lines for model-based computations). This is an example of a truncated O-wave trace cusp near the critical frequency, foF2. The MH Digisonde is not authorized to transmit HF frequencies in the band from 6.2 to 6.8 MHz (restricted frequencies). All restricted frequencies are marked by a black underscore line along the frequency axis. The left table enlists standard URSI-specified characteristics derived from the ionogram image.

The bottomside ionograms on SAOExplorer were inspected and manually scaled to produce reliable bottomside electron density profiles as in Figure 4. The MH Digisonde transmissions are restricted in several frequency intervals indicated by a black underscore line in Figure 4, which sometimes results in truncating the X or O trace cusps in the vicinity of the critical frequency. Yet, one of the O- and X-wave cusps is well-defined in the ionograms, allowing the other cusp to be restored by replication, given that the separation of the foF2 and fxF2 is equal to the half-gyrofrequency. Careful manual inspection of the ionograms for this case-by-case investigation ensured a good quality of the bottomside electron density profiles.

3 Recalibrating Ion-Line Profile using Peak Density N_mF2

Inspection of different MH-ISR modes on June 22, 2016, showed that, in most cases, the ISR ion acoustic N_mF2 is greater than the ISR plasma line N_mF2 due to a systematic calibration offset, in this data set, in the ISR ion acoustic electron density profiles (Figure 5). ISR plasma line N_mF2 measurements are only available in the daytime due to the need for the presence of photoelectrons, hence the values of the ISR plasma line N_mF2 during nighttime are set to zero.

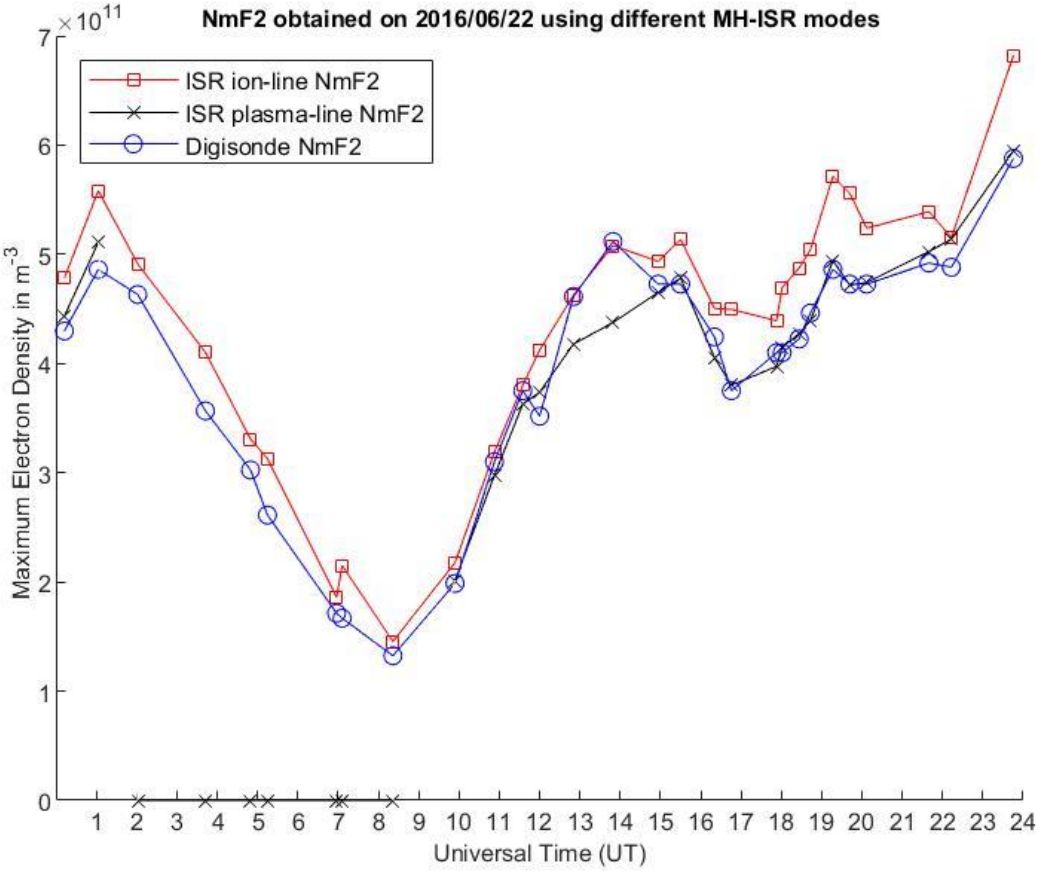

Figure 5. N_mF2 values obtained from 29 profiles on June 22, 2016 using ISR ion acoustic density measurements (red squares), Digisonde measurements (blue circles), and ISR plasma line measurements (black x). Plasma line N_mF2 values have good agreement with Digisonde N_mF2 values. N_mF2 values obtained from ISR ion acoustic electron density profiles are slightly greater than N_mF2 values obtained from both the plasma line and the Digisonde measurements.

4 The Peak Density Thickness in MH-ISR profiles

The MH-ISR-provided joint bottomside and topside measurements consistently show the presence of an altitude interval around the peak density N_mF2 where the observed density *N(h)* remains constant until it starts decreasing into the topside part of the ionosphere. We describe this ‘broad peak’ or ‘flat-nose’ property of the density profile shape as the Peak Density Thickness (PDT) parameter χ (Figure 6). The start point of the PDT is determined when the plasma line intersects with the error bars of the "recalibrated" ion line profile (similar to Figure

3b and Figure 3d) and ends at the highest intersection between the MH-ISR plasma-line N_mF2 and the recalibrated ion-line profile *N(h)*.

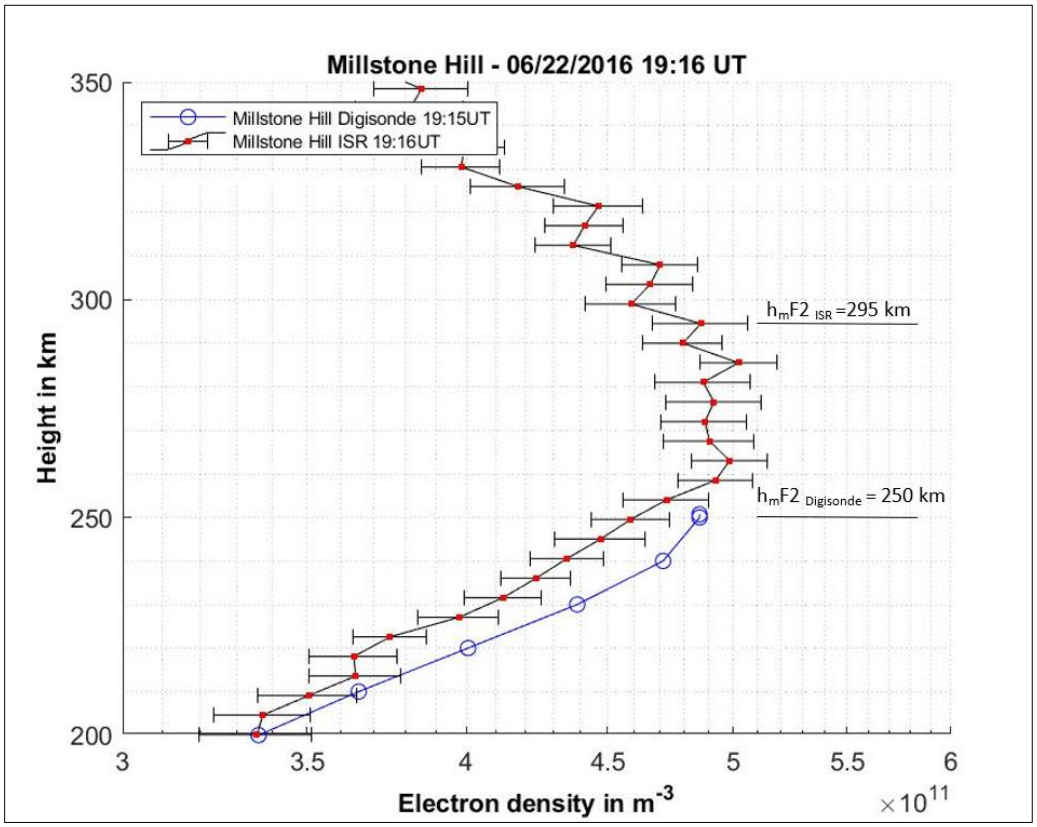

Figure 6. The combined ionosonde-derived (blue circles) and ISR-derived (red squares) measurements show a flat nose F2 peak with a Peak Density Thickness χ= 36 km. In this particular example, both Digisonde and ISR have considerably different F2 peak heights; h_mF2$_{ISR}$ is measured by ISR, and h_mF2$_{Digi}$ is measured by the Digisonde (in this paper, h_mF2 without a subscript also refers to h_mF2$_{Digi}$).

Figure 7 shows computed PDT values on June 22, 2016 (blue line) versus the Digisonde-provided standard IRI parameter B0 (Bilitza, 1990) that can be interpreted as a measure of the sub-peak F2 layer thickness:

$$N(h)/N_m\text{F2} = \exp(-X^{B1})/\cosh(X) \qquad (1)$$

$$\text{with} \qquad X = (h_m\text{F2}-h)/\text{B0}$$

In Figure 7, B0 is plotted scaled by a factor of ¼ in order to fit the chart. PDT has minimum values during nighttime and reaches its maximum at the local solar noon. The comparison reveals a correlation between the PDT parameter and the Digisonde B0 parameter.

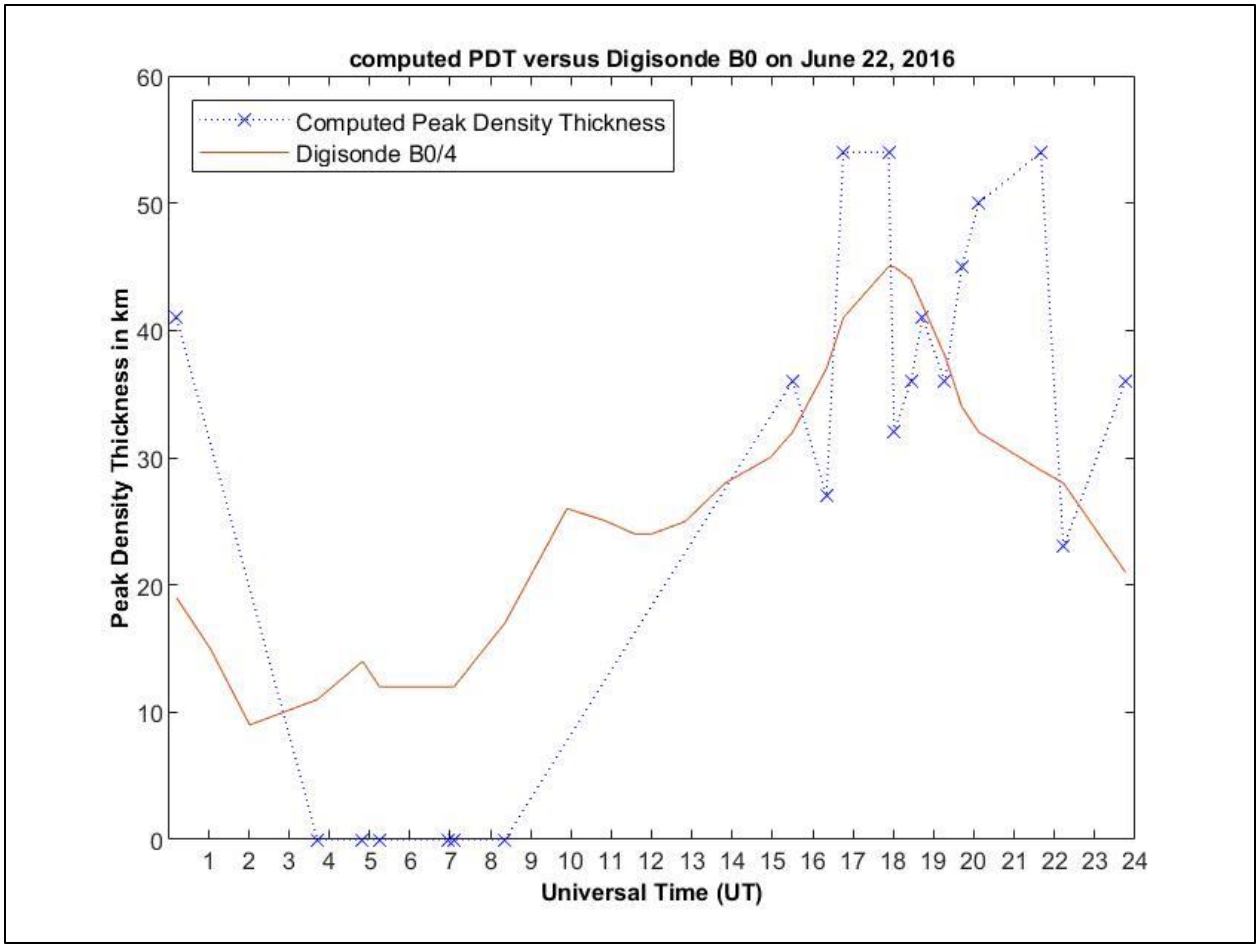

Figure 7. The red line represents B0/4 where B0 is the Digisonde bottomside thickness parameter and the blue line represents the measured PDT values. Data from June 22nd, 2016

5 Discussion

Proposed addition of the flat-nose PDT segment to the $N(h)$ profile specification will improve the accuracy of the electron density characterization by the "Digisonde-assisted" class of topside ionosphere models (Reinisch and Huang., 2001, 2004a,b; Kutiev et al., 2009; Belehaki et al., 2012) that use the sub-peak $N(h)$ shape measurements to constrain the model representation of the super-peak plasma. If the Digisonde-assisted models take into account the altitude gap χ between the bottomside and the topside F2 layer profile, their improved agreement with the MH-ISR measurement is expected, as illustrated in Figure 8 where the Vary-Chap topside ionosphere model (Nsumei et al. 2012), is provided with additional PDT segment.

Figure 8 shows the Vary-Chap topside profile using Nsumei's model-parameters values of the summer season at Millstone Hill, adopted from Nsumei et al. [2012]. The figure also shows the simultaneous measurements of the Millstone Hill Digisonde bottomside profile and the ISR topside profile. The thin blue line shows the Vary-Chap profile starting from the F2 layer peak height h_mF2 while the crossed blue line shows the Vary-Chap profile starting from $h_mF2 + \chi$. The Vary-Chap model and the ISR topside measurements agree better when the PDT of the

F2 layer is considered. In this example, the peak density thickness starts at the Digisonde peak height h_mF2_{Digi} and ends at the height where the ISR N_mF2 density starts to decline.

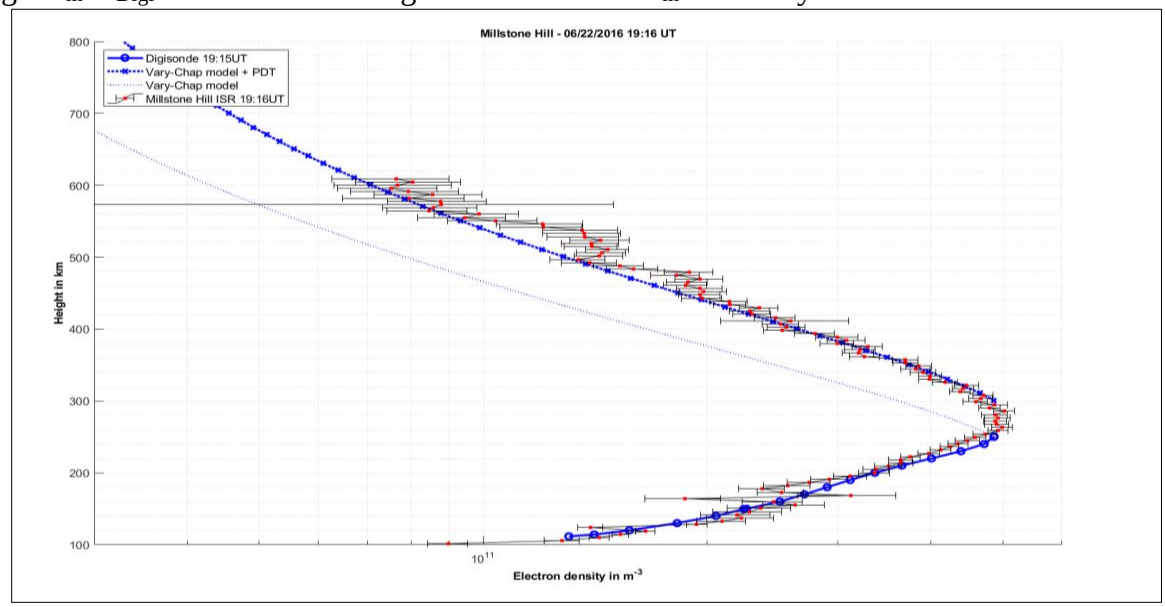

Figure 8. Combined measurement of *N(h)* profile using MH ISR and Digisonde, same as in Figure 6, with the superimposed topside Vary-Chap model before (thin blue line) and after (crossed blue line) addition of the PDT segment χ. The PDT-augmented topside Vary-Chap profile starts from $h_mF2 + \chi$ rather than h_mF2, thus bringing the topside profile representation into good agreement with the ISR measurements.

A brief review of our selection of the Vary-Chap topside profile model for this investigation is warranted in order to explain how PDT is added to the formalism. Indeed, many efforts have been made to address the problem of finding suitable functions for the topside electron density profile, e.g., exponential (Llewellyn and Bent 1973; Stankov et al. 2003), sech-squared (Kutiev and Marinov 2007), semi-Epstein (Themens et al. 2018; Depuev and Pulinets 2004; Radicella and Leitinger 2001; Rawer 1988), a combination of multi-layer Epstein functions with constant scale heights for O+ and H+ (Sibanda and McKinnell 2011). Fonda et al. (2005) compared different functions for the topside ionosphere and concluded that Chapman functions are most suitable in describing the topside profile. Many efforts were made to describe the topside profile using a single-layer Chapman function (Chapman 1931; Reinisch et al., 2004; McNamara et al., 2007; Tulasi Ram et al., 2009; Venkatesh et al. 2011), a combination of multi-layer Chapman functions with constant scale heights for O+ and H+ [e.g., Kutiev et al., 2006], a combination of multi-layer Chapman functions with a constant scale heights for O+, and a linear varying scale height for H+ and He+ ions (Zhu et al. 2015), a single layer Chapman function with a linear varying scale height (Hernández-Pajares et al. 2017) or a tangential varying scale height (Reinisch et al. 2007). Reinisch et al. [2007] used the general Chapman function [Rishbeth and Garriott, 1969], which allows the scale height to vary continuously with height resulting in the "Vary-Chap" profile,

$$\frac{N(h)}{N_m} = \left[\frac{H(h)}{H_m}\right]^{-1/2} \exp\left\{\frac{1}{2}[1 - Y - \exp(Y)]\right\} \quad \text{where } Y = \int_{h_m}^{h} \frac{dh}{H(h)} \tag{2}$$

where N_m, H_m, and h_m are the density, scale height, and height, respectively, of the F2 layer peak and $H(h)$ is the scale height. This previous analysis suggests the use of the scale height value H_m at the F2 peak derived from the bottomside profile for the construction of the topside normalized scale height function $H(h)/H_m$ (Reinisch et al., 2007; Bilitza et al., 2011). This approach led to unsatisfactory results [Kutiev et al., 2009], and therefore, Nsumei et al. [2012] used the same Vary-Chap technique and replaced $H(h)/H_m$ by a shape function $S(h)$:

$$N(h) = N_m \left[S(h)\right]^{-1/2} \exp\left\{\frac{1}{2}\left[1 - Y - \exp\left(Y\right)\right]\right\}, \quad (3)$$

$$\text{where} \quad Y(h) = \frac{1}{h_m}\int_{h_m}^{h} \frac{dh}{S(h)}$$

Nsumei et al. [2012] used a parametrized shape function $S(h)$ that is specified by three parameters α, β, and h_T:

$$\frac{1}{S(h)} = \frac{1}{c_1}\,\mathrm{sech}^2\left(\frac{z-1}{\beta/h_m}\right) + \frac{1}{c_2}\frac{z}{(1+z^2)^{\alpha}} \quad (4)$$

where h_m is the F2 layer peak height h_mF2. The transition height parameter h_T is used in the boundary condition that governs C1 and C2. $z = h/h_m$ where h is the independent variable of height.

The current study adopts Nsumei et al. [2012] Vary-Chap profile, but instead of using h_mF2 to reconstruct the topside profile, the current study uses the sum of the peak height h_mF2 and the Peak Density Thickness (PDT) χ. Hence, the Vary-Chap equation becomes:

$$N(h) = N_m \left[S(h)\right]^{-1/2} \exp\left\{\frac{1}{2}\left[1 - Y - \exp\left(Y\right)\right]\right\} \quad (5)$$

$$\text{where} \quad Y = \frac{1}{h_{PDT}}\int_{h_{PDT}}^{h} \frac{dh}{S(h)}$$

here $h_{PDT} = h_mF2 + \chi$ and χ is the Peak Density Thickness (PDT).

The parameterized shape function S(h) is now specified by four rather than three parameters: α, β, h_T and χ:

$$\frac{1}{S(h)} = \frac{1}{c_1}\,\mathrm{sech}^2\left(\frac{z-1}{\beta/h_{PDT}}\right) + \frac{1}{c_2}\frac{z}{(1+z^2)^{\alpha}} \quad (6)$$

Figure 9 shows other examples of simultaneous Millstone Hill Digisonde bottomside profile and the ISR topside profile measurements. We fitted the parametrized Vary-Chap function to the ISR topside profile using Least Square Fitting (LSF), and started the Vary-Chap profile from $h_mF2_{ISR} \sim= h_mF2 + \chi$. The start point of the PDT is determined when the plasma line intersects with the error bars of the "recalibrated" ion line profile (similar to figure 3b and figure 3d). The endpoint of the PDT is determined when the plasma line is no longer within the error bars of the ion line profile.

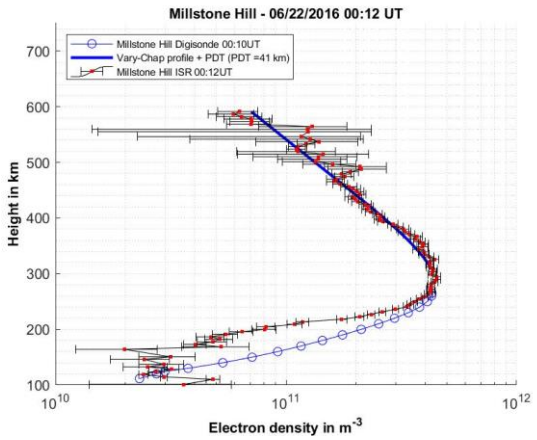
Millstone Hill - 06/22/2016 00:12 UT
Millstone Hill Digisonde 00:10UT
Vary-Chap profile + PDT (PDT =41 km)
Millstone Hill ISR 00:12UT
Height in km
Electron density in m-3

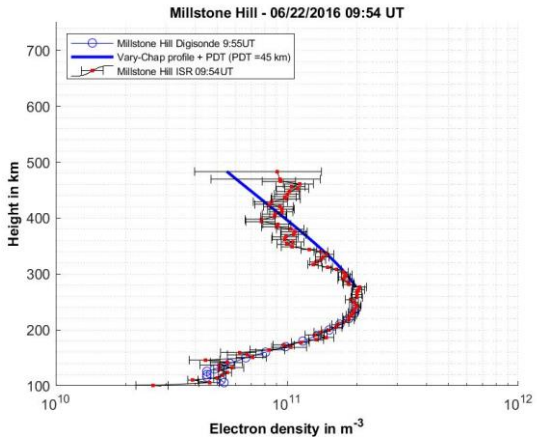
Millstone Hill - 06/22/2016 09:54 UT
Millstone Hill Digisonde 9:55UT
Vary-Chap profile + PDT (PDT =45 km)
Millstone Hill ISR 09:54UT
Height in km
Electron density in m-3

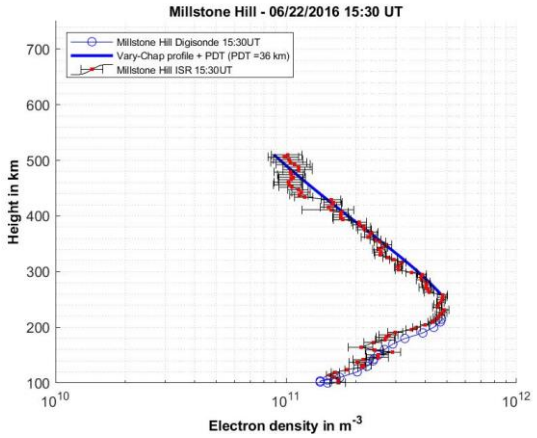
Millstone Hill - 06/22/2016 15:30 UT
Millstone Hill Digisonde 15:30UT
Vary-Chap profile + PDT (PDT =36 km)
Millstone Hill ISR 15:30UT
Height in km
Electron density in m-3

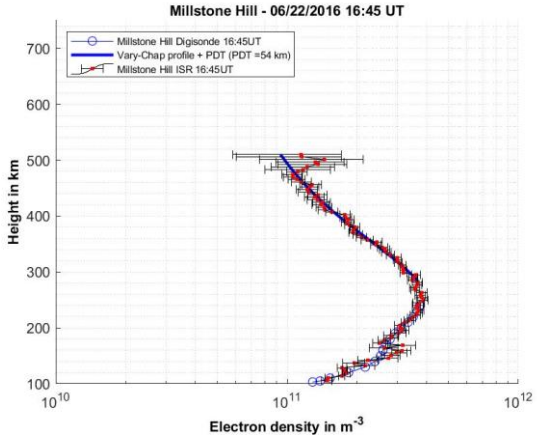
Millstone Hill - 06/22/2016 16:45 UT
Millstone Hill Digisonde 16:45UT
Vary-Chap profile + PDT (PDT =54 km)
Millstone Hill ISR 16:45UT
Height in km
Electron density in m-3

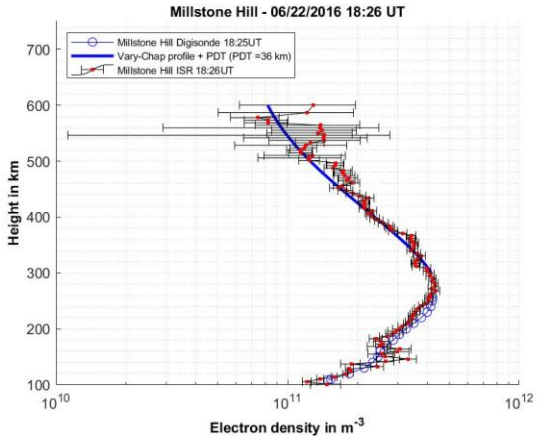
Millstone Hill - 06/22/2016 18:26 UT
Millstone Hill Digisonde 18:25UT
Vary-Chap profile + PDT (PDT =36 km)
Millstone Hill ISR 18:26UT
Height in km
Electron density in m-3

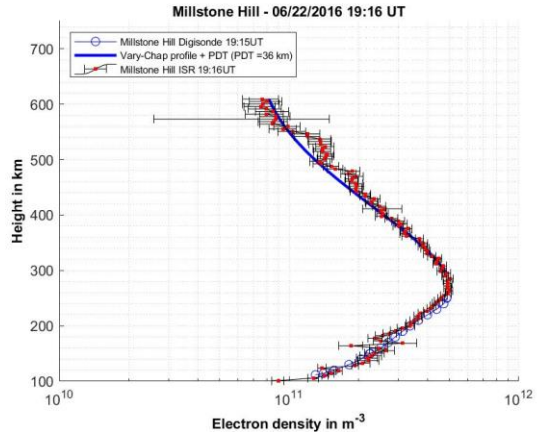
Millstone Hill - 06/22/2016 19:16 UT
Millstone Hill Digisonde 19:15UT
Vary-Chap profile + PDT (PDT =36 km)
Millstone Hill ISR 19:16UT
Height in km
Electron density in m-3

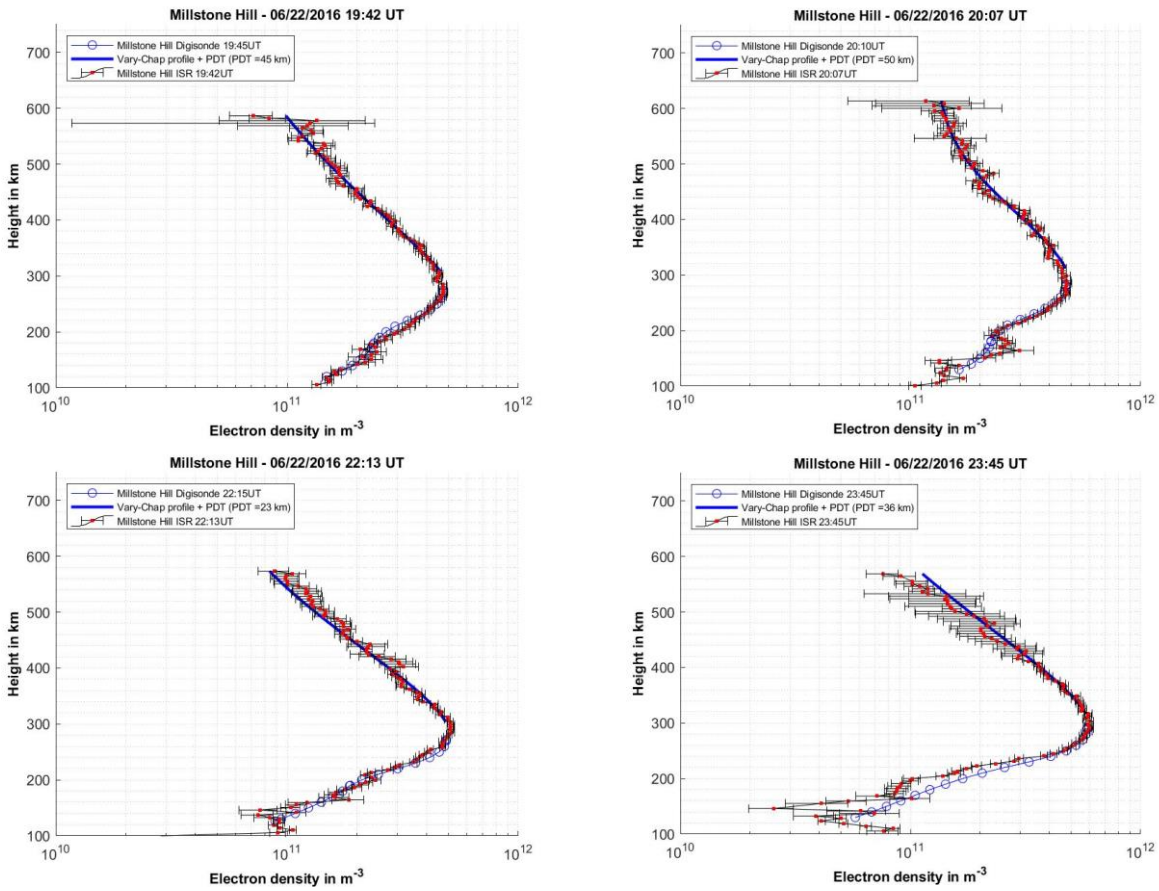

Figure 9. The Vary-Chap profile starts at h_mF2_{ISR}~= h_mF2+ PDT (blue line) and is fitted to the ISR ion acoustic profile (red squares) that has been elastically transformed to match it to the ISR plasma line N_mF2. The simultaneous Digisonde measurement (blue circles) is also plotted and used to obtain N_mF2 and h_mF2. Measurements were recorded on June 22nd, 2016.

6 Conclusion

Simultaneous measurements of the electron density profile using the Millstone Hill Digisonde and the Incoherent Scatter Radar (ISR) at MIT Haystack Observatory suggest the profile shape around the F2 peak density is flat with a peak density thickness that varies during the 24 hours. Results suggest the F2 Peak Density Thickness PDT has a diurnal correlation with the Digisonde bottomside thickness parameter B0. In this research, we reconstructed the Millstone Hill ISR topside profile using a Vary-Chap function combined with the Peak Density Thickness PDT parameter. The results suggest the PDT parameter can be approximated by B0/4 where B0 is taken from the Digisonde measurements. Therefore, ground-based Digisondes measurements can be reliably used to construct the density profile between the bottomside and the topside electron density profiles.

Future work should involve applying the Vary-Chap technique combined with the PDT parameter during different geomagnetic and solar conditions. Also, we suggest investigating simultaneous measurements of co-located Digisondes and ISRs at equatorial and high latitudes.

Acknowledgments

The Millstone Hill Digisonde database is available over the GIRO Web Portal, http://giro.uml.edu, and the Millstone Hill ISR data is accessible through the Madrigal database, https://millstonehill.haystack.mit.edu. Operations and community database access at Millstone Hill for the observations in this study were supported by US National Science Foundation grant AGS-1952737 to the Massachusetts Institute of Technology.

References

Belehaki, A., I. Kutiev, B. Reinisch, N. Jakowski, P. Marinov, I. Galkin, C. Mayer, I. Tsagouri,and T. Herekakis (2012), Verification of the TSMP-assisted Digisonde topside profiling technique. *Acta Geophysica*, 58, 432-452. doi:10.2478/s11600-009-0052-3

Bilitza, D. (1990), International reference ionosphere 1990, NSSDC/ WDC-A-R&S 90-22. National Space Science Data Center, Greenbelt

Bilitza, D., L.-A. McKinnell, B. Reinisch, and T. Fuller-Rowell (2011), The International Reference Ionosphere (IRI) today and in the future, J. Geod., 85, 909–920. doi:10.1007/s00190-010-0427-x

Chapman S. (1931), The absorption and dissociative or ionizing effect of monochromatic radiation in an atmosphere on a rotating Earth. *Proc Phys Soc* 43:26–45

Croft, T. A. and H. Hoogansian (1968), Exact Ray Calculations in a Quasi-Parabolic Ionosphere With No Magnetic Field. *Radio Science*, 3. https:doi: 10.1002/rds19683169

Depuev V. H, Pulinets S.A. (2004), A global empirical model of the ionospheric topside electron density. *Adv Space Res* 34:2016–2020

Evans, J.V. (1965), Ionospheric backscatter observations at Millstone Hill. *Planetary and Space Science*, 13(11). doi: 10.1016/0032-0633(65)90138-8

Erickson, P. J., Observations of light ions in the midlatitude and equatorial topside ionosphere, Cornell University, 1998.

Erickson, P. J., (2012), ISR, TEC, and SuperDARN capabilities at subauroral latitudes: RBSP coordinated science, *Proc. RBSP SWG IT*, JHUAPL, John Hopkins University, available at: rbspgway.jhuapl.edu/sites/default/files/20120820/SWG_IT_Session/Erickson_SWG_IT_Inocoh_Radars_21Aug12.pdf.

Fleming, J.A. (1902), Waves and Ripples in Water, Air, and Ether. *Proc. Royal Institution of Great Britain, 17*, 223.

Fonda, C., P. Coisson, B. Nava, and S. M. Radicella (2005), Comparison of analytical functions used to describe topside electron density profiles with satellite data. *Ann. Geophys.*, 48(3), 491–495.

Galkin, I.A., B.W. Reinisch, D. Bilitza (2018), Realistic Ionosphere: real-time ionosonde service for ISWI. *Sun and Geosphere, 2018; 13/2: 173-178, ISSN 2367-8852*

Hernández-Pajares M, Garcia-Fernàndez M, Rius A, Notarpietro R, von Engeln A, Olivares-Pulido G (2017), Electron density extrapolation above F2 peak by the Linear Vary-Chap model supporting new global navigation satellite systems-LEO occultation missions. *J Geophys Res Space Phys* 122:9003–9014

Holt, J. M. (2008), A new High-level Gridded Madrigal Data Product for IPY Incoherent Scatter Radar Data and Model Output. *Abstracts of AGU Fall Meeting 2008*, SA33B-1634, ADS: 2008AGUFMSA33B1634H.

Jackson, J. E., E. R. Schmerling, and J. H. Whitteker (1980), Mini-review on topside sounding. *IEEE Trans. Antennas Propag.*, 28, 284–288. doi:10.1109/TAP.1980.1142318

Khmyrov, G. M., I. A. Galkin, A. V. Kozlov, B. W. Reinisch, J. McElroy, and C. Dozois, Exploring digisonde ionogram data with SAO-X and DIDBase. in *Radio Sounding and Plasma Physics, AIP Conf. Proc. 974*, 175-185, 2008.

Kutiev, I., and P. Marinov (2007), Topside sounder model of scale height and transition height characteristics of the ionosphere. *Adv. Space Res.*, 39, 759–766. doi:10.1016/j.asr.2006.06.013

Kutiev, I. S., P. G. Marinov, and S. Watanabe (2006), Model of topside ionosphere scale height based on topside sounder data, Adv. *Space Res.*, 37, 943–950. doi:10.1016/j.asr.2005.11.021

Kutiev, I., P. Marinov, A. Belehaki, B. Reinisch, and N. Jakowski (2009), Reconstruction of topside density profile by using the topside sounder model profiler and Digisonde data. *Adv. Space Res.*, 43, 1683–1687. doi:10.1016/j.asr.2008.08.017

Lehtinen, M. S., and Häggström, I. (1987), A new modulation principle for incoherent scatter measurements, *Radio Sci.*, 22(4), 625– 634, doi:10.1029/RS022i004p00625.

Llewellyn, S. K., and R. B. Bent (1973), Documentation and description of the Bent Ionospheric Model. Rep. AFCRL-TR-73-0657, Hanscom AFB, Mass.

McNamara, L. F., D. L. Cooke, C. E. Valladares, and B. W. Reinisch (2007), Comparison of CHAMP and Digisonde plasma frequencies at Jicamarca. *Peru, Radio Sci.*, 42, RS2005. doi:10.1029/2006RS003491

Nsumei, P., B. W. Reinisch, X. Huang, and D. Bilitza (2010), Comparing topside and bottomside-measured characteristics of the F2 layer peak. *Adv. Space Res.*, 46, 974-983. doi:10.1016/j.asr.2010.06.027

Nsumei, P., B. W. Reinisch, X. Huang, and D. Bilitza (2012), New Vary-Chap profile of the topside ionosphere electron density distribution for use with the IRI model and the GIRO real time data. *Radio Sci.*, 47, RS0L16, doi:10.1029/2012RS004989.

Radicella, S. M., and R. Leitinger (2001), The evolution of the DGR approach to model electron density profiles. *Adv. Space Res.*, 27(1), 35–40. doi:10.1016/S0273-1177(00)00138-1

Rawer, K. (1988), Synthesis of ionospheric electron density profiles with Epstein functions. *Adv. Space Res.*, 8(4), 191–199. doi:10.1016/0273-1177(88)90239-6

Reinisch, B. W. and I. A. Galkin (2011), Global Ionospheric Radio Observatory (GIRO), *Earth Planets Space*, 63(4), pp. 377-381. doi:10.5047/eps.2011.03.001

Reinisch, B.W., Huang, X. Deducing topside profiles and total electron content from bottomside ionograms. *Adv. Space Res.* 27(1), 23–30, 2001.

Reinisch, B. W., X. Huang, A. Belehaki, J. Shi, M. L. Zhang, and R. Ilma (2004a), Modeling the IRI topside profile using scale heights from groundbased ionosonde measurements. *Adv. Space Res.*, *34*, 2026–2031. doi:10.1016/j.asr.2004.06.012

Reinisch, B. W., Huang X., A. Belehaki, and R. Ilma (2004b), Using scale heights derived from bottomside ionograms for modeling the IRI topside profile. *Adv. Radio Sci.*, 2, 293-297. doi: 10.5194/ars-2-293-2004

Reinisch, B. W., P. Nsumei, X. Huang, and D. K. Bilitza (2007), Modeling the F2 topside and plasmasphere for IRI using IMAGE/RPI, and ISIS data. *Adv. Space Res.*, 39, 731–738. doi:10.1016/j.asr.2006.05.032

Reinisch, B. W., et al. (2009), New Digisonde for research and monitoring applications. *Radio Sci.*, 44, RS0A24. doi:10.1029/2008RS004115

Rishbeth, H., and O. K. Garriott (1969), Introduction to Ionospheric Physics. *Academic, New York*

Sibanda P, McKinnel LA (2011) Topside ionospheric vertical electron density profile reconstruction using GPS and ionosonde data: possibilities for South Africa. *Ann Geophys*, 29:229–236

Showen, R. L. (1979), The spectral measurement of plasma lines. *Radio Science*, *14*(3). doi: 10.1029/RS014i003p00503

Stankov SM, Jakowski N, Heise S, Muhtarov P, Kutiev I, Warnant R (2003), A new method for reconstruction of the vertical electron density distribution in the upper ionosphere and plasmasphere. *J Geophys Res*, 108:1164

Themens DR, Jayachandran PT, Bilitza D, Erickson PJ, Häggström I, Lyashenko MV, Reid B, Varney RH, Pustovalova L (2018), Topside electron density representations for middle and high latitudes: a topside parameterization for E-CHAIM based on the NeQuick. *J Geophys Res Space Phys*, 123:1603–1617

Tulasi Ram, S., S.-Y. Su, C. H. Liu, B. W. Reinisch, and L.-A. McKinnell (2009), Topside ionospheric effective scale heights (HT) derived with ROCSAT-1 and ground-based ionosonde

observations at equatorial and midlatitude stations. *J. Geophys. Res.,* 114, A10309. doi:10.1029/2009JA014485

Venkatesh K, Rama Rao PVS, Saranya PL, Prasad DSVVD, Niranjan K (2011), Vertical electron density and topside effective scale height (HT) variations over the Indian equatorial and low latitude stations. *Ann Geophys*, 29:1861–1872

Zhu J, Zhao B, Wan W, Ning B, Zhang S (2015), A new topside profiler based on Alouette/ISIS topside sounding. *Adv Space Res,* 56:2080–2090